Tracking a Maneuvering Target by Multiple Sensors Using Extended Kalman Filter with Nested Probabilistic-Numerical Linguistic Information

Xinxin Wang, *Student Member, IEEE*, Zeshui Xu, *Fellow, IEEE*, Xunjie Gou, *Student Member, IEEE*, Ljiljana Trajkovic, *Fellow, IEEE*

Abstract—**Tracking a maneuvering target is an important technology in real life. However, due to complex environment and diversity of sensors, sensors' errors need to be optimized with respect to various motion states during the tracing process. In this paper, we first propose how to unify the coordinate system and data preprocessing in case of tracking using multiple–sensors. We then combine fuzzy sets with a novel trace optimization method based on extended Kalman filter with nested probabilistic–numerical linguistic information. We present a case study of trace optimization of an unknown maneuvering target in Sichuan province in China. We solve the case by using both the proposed method and the traditional extended Kalman filter and offer comparative analysis to validate the proposed approach.**

Index Terms—**Tracking maneuvering target, extended Kalman filter, nested probabilistic-numerical linguistic information, trace optimization**

I. INTRODUCTION

Tracking a maneuvering target is an indispensable technology in modern information systems and greatly contributes to the civilian applications [1]–[3]. The objective of the tracking is to estimate the states based on the noisy observations by sensors. The key to its successful deployment depends on the effective and accurate extraction of useful information. Difficulties in tracking the maneuvering target are due to the complex tracking process and include: (1) accurately establishing the maneuvering target's state equation (The tracking target is usually non–cooperative [4] and it may be difficult to accurately describe the speed and direction of the target.) and (2) dealing with sensor's systemic error [5]. In addition to outside interference, the measurement information received from the sensor such as distance, azimuth angle, and pitch angle involve a certain amount of random error, which makes it difficult to accurately estimate the characteristics of the maneuvering target. These challenges make tracking a maneuvering target an interesting and difficult research topic [6]–[7].

Several popular estimation techniques have been proposed to address tracking a maneuvering target. They include nonlinear least squares [8], Kalman filter (KF) [5], and extended Kalman filter (EKF) [9]–[10]. Since KF is unbiased and linear, it is a conventional option for estimating the system behavior. Moreover, since it has a minimum error variance of the unknown state vector, it is used as an optimal recursive data processing algorithm in many fields and applications [11]–[12]. Nevertheless, due to the limitations of tracking tools and the complex environment in practice, KF is easily affected by noise, which leads to its divergence in case of Gaussian noise. Since the observation equation of the maneuvering target is usually nonlinear, the KF algorithm developed for the optimal minimum-variance state estimation in linear discrete-time Gaussian models may not be applicable. Several research studies have combined linearization and discretization of a given stochastic systems by applying the standard KF technique [13]–[15]. Popular filters dealing with nonlinear systems include EKF, unscented Kalman filter (UKF), and cubature Kalman filter (CKF). The EKF algorithm is considered to be the simplest and suboptimal but a successful state estimator to handle nonlinear systems. It has been used in applied science and engineering for decades [16]–[18]. In case of systems with high nonlinearities, the UKF algorithm is constraints on Gaussian noise and the timeliness is relatively poor compared with EFK algorithm [10]. The heart of the CKF is a spherical-radial cubature rule, which makes it possible to numerically compute multivariate moment integrals of the nonlinear Bayesian filter. While the CKF may provide a systematic solution for high-dimensional nonlinear filtering problems, it is unsuitable for the tracking applications [19].

When the motion state of the maneuvering target and the detection environment are complex and lack information regarding the model or noise statistics, the target tracking problems are based on fuzzy set theory [20]. For example, after

X. X. Wang is with the Business School, Sichuan University, Chengdu 610064, China (e–mail: wangxinxin_cd@163.com).
Z. S. Xu is with the Business School, Sichuan University, Chengdu 610064, China (e–mail: xuzeshui@263.net).
X. J. Gou is with the Business School, Sichuan University, Chengdu 610064, China and Department of Computer Science and Artificial Intelligence, University of Granada, Granada 18071, Spain (e–mail: gou_xunjie@163.com).
Lj. Trajkovic is with the School of Engineering Science, Simon Fraser University, Burnaby, BC V5A 1S6, Canada (e–mail: ljilja@cs.sfu.ca).

training fuzzy systems with KF and EKF, fuzzy Kalman filtering with Takagi-Sugeno rules coincides with discrete Kalman filtering equations [21]–[22]. The validity domains of sensors are defined using fuzzy sets [23] while the KF and Takagi-Sugeno fuzzy modeling technique are combined to extend the classical Kalman linear state estimation to the nonlinear system [24]. These methods have been widely used in applications such as dynamic mobile localization [25], truck backing-up problems [26], and trajectory tracking control [27].

Even though extended methods combined with fuzzy set theory, such as fuzzy KF or fuzzy EKF, are popular when dealing with target tracking problems, they have two main limitations: (1) the estimation of the motion states is important for tracking the maneuvering target during the entire tracking process because it directly impacts the parameters of the observation equation [28]–[29]. However, the existing methods estimate the motion states based on the speed and direction of the maneuvering target during a short period of time by using acceleration as a measure. This approach is imprecise due to a number of complex factors that impact the motion state, and (2) the error parameters in the tracking process are the systemic sensor's errors as the largest error contributors. These error parameters vary with motion states of the maneuvering target because there are multiple motion states during the tracking process. Since it would be inaccurate to adopt the systemic error parameters of the sensor to optimize the trace during the entire process, it is necessary to optimize them over a number of motion states during the tracking process.

In this paper, we improve the current approaches for tracking a maneuvering target. Difficulties in estimating the motion state when the sensor detects the maneuvering target call for evaluation of the quantitative (acceleration) and qualitative (location and current trace) information. Combined with fuzzy set theory, the linguistic terms are closer to human cognitive processes and the fuzzy linguistic approaches such as virtual linguistic term model [30], hesitant fuzzy linguistic term set (HFLTS) [31], and probabilistic linguistic term set (PLTS) [32]. They are considered to be the best choices [33] and have achieved superior results in many fields and applications [34]–[36]. These fuzzy linguistic methods deal well with qualitative problems. However, the process of optimizing tracking of the maneuvering target involves both quantitative and qualitative information. For example, the trajectory shape of a maneuvering target needs to be evaluated and the systemic error of the sensor under various motion states needs to be reduced. The nested probabilistic–numerical linguistic term set (NPNLTS) [37] simultaneously deals with the quantitative and qualitative information. It helps obtain more accurate results and deal with the optimization problems that represent nested information and contain both probabilistic and numerical information [38-39]. In this paper, we propose a novel trace optimization method based on EKF with nested probabilistic-numerical linguistic information to deal with tracking a maneuvering target.

Compared to the existing approaches, the contributions of this paper are:

- Using NPNLTS to optimize sensor's errors in various motion states of the maneuvering target. NPNLST considers both quantitative and qualitative information to obtain precise error parameters.
- Using the trace optimization of the maneuvering target based on EKF with nested probabilistic–numerical linguistic information to reduce the errors caused by uncertain motion states in a nonlinear system.

The remaining of this paper is organized as follows: Section II introduces basic NPNLTS and EKF concepts. In Section III, we propose a trace optimization method based on EKF with nested probabilistic–numerical linguistic information and the corresponding algorithm. A case study for trace optimization of unknown maneuvering target in Sichuan province in China is described in Section IV. Finally, comparative analysis and discussion regarding the proposed and the EKF methods are given in Section V. We conclude with Section VI.

II. PRELIMINARIES

We first review NPNLTS concepts and operations as well as the rationale for using the EKF.

A. Nested probabilistic–numerical linguistic term set

Based on PLTS [32] and other existing techniques, the NPNLTS is defined as $NPN = \{OL(p)\{IL(v)\}\}$ [37]. It consists of outer-layer and inner-layer probabilistic linguistic term sets (OPLTS) $OL(p)$ and (INLTS) $IL(v)$, respectively:

$$OL(p) = \left\{ \begin{array}{l} OL^{(k)}\left(p^{(k)}\right) \mid OL^{(k)} \in OS,\ p^{(k)} \geq 0, \\ k = 1, 2, \cdots, \#OL(p),\ \sum_{k=1}^{\#OL(p)} p^{(k)} \leq 1 \end{array} \right\} \quad (1)$$

and

$$IL(v) = \left\{ IL^{(l)}\left(v^{(l)}\right) \mid IL^{(l)} \in IS,\ v^{(l)} \geq 0, l = 1, 2, \cdots, \#IL(v) \right\}, \quad (2)$$

where in the nested linguistic term set (NLTS), $OS = \{s_\alpha \mid \alpha = 0, 1, 2, \cdots, \tau\}$ and $IS = \{n_\beta \mid \beta = 0, 1, 2, \cdots, \varsigma\}$ are an outer-layer (OLTS) and an inner-layer (ILTS) linguistic term sets, respectively. The term $OL^{(k)}\left(p^{(k)}\right)$ is the k-th outer-layer linguistic term element (OLTE) in the OLTS associated with the probability $p^{(k)}$ while $\#OL(p)$ is the number of the linguistic term elements in $OL(p)$. The term $IL^{(l)}\left(v^{(l)}\right)$ is the l-th inner-layer linguistic term element (ILTE) in the ILTS associated with the value $v^{(l)}$ while $\#IL(v)$ is the number of the linguistic term elements in $IL(v)$.

The corresponding normalized NPNLTS (N–NPNLTS) [37] is denoted as $\overline{NPN} = \left\{ OL^N(p)\{IL^N(v)\} \right\}$, where:

$$OL^N(p) = \left\{ \begin{array}{l} OL^{N(k)}\left(p^{N(k)}\right) \mid OL^{N(k)} \in OS,\ p^{N(k)} \geq 0, \\ k = 1, 2, \cdots, \tau + 1, \sum_{k=1}^{\tau+1} p^{N(k)} = 1 \end{array} \right\}. \quad (3)$$

$$IL^N(v) = \left\{ IL^{N(l)}\left(v^{N(l)}\right) \mid IL^{N(l)} \in IS,\ v^{N(l)} \geq 0\ or\ '-', l = 1, 2, \cdots, \varsigma + 1 \right\}, \quad (4)$$

$p^{N(k)} = p^{(k)} \Big/ \sum_{k=1}^{\tau+1} p^{(k)}$, and $v^{N(l)} = v^{(l)} \Big/ \sum v^{(l)}$. The entire score function of NPNLTS is defined as: $F(NPN) = \sum_{l=1}^{\#IL(v)}\left(\bar{v}^{(l)}\right)\Big/\#IL(v)$, where $\bar{v}^{(l)} = \left(\lceil\bar{\alpha}\rceil - \bar{\alpha}\right)\times IL_{(\lfloor\bar{\alpha}\rfloor)}\left(v^{(l)}\right) + \left(\bar{\alpha} - \lfloor\bar{\alpha}\rfloor\right)\times IL_{(\lceil\bar{\alpha}\rceil)}\left(v^{(l)}\right)$, $\bar{\alpha} = \sum_{k=1}^{\#OL(p)} r^{(k)}p^{(k)} \Big/ \sum_{k=1}^{\#OL(p)} p^{(k)}$, $r^{(k)}$ is the subscript of the k-th linguistic term $OL^{(k)}$, $\lceil\bar{\alpha}\rceil$ is the smallest integer greater than $\bar{\alpha}$, and $\lfloor\bar{\alpha}\rfloor$ is the greatest integer smaller than $\bar{\alpha}$. The deviation degree of NPNLTS is:

$$\sigma(NPN) = \left(\sum_{l=1}^{\#IL(v)}\left(v^{(l)} - F(NPN)\right)^2 \Big/ \#IL(v)\right)^{1/2} .$$

B. Extended Kalman Filter

The Kalman filter algorithm is a popular method for the state estimation of linear systems [12]. The EKF algorithm was later proposed to deal with nonlinear systems in numerous fields [16]–[18]. Considering the nonlinear system in discrete time, the state and the observation vectors may be expressed as:

$$X(k) = f(k, X(k-1)) + w(k), \quad (5)$$
$$Z(k) = h(k, X(k)) + v(k)$$

where $X(k)$ and $Z(k)$ are the state and observation vectors at time k , respectively, f is the nonlinear function, h is the first order continuous partial derivative, and $w(k)$ and $v(k)$ are the process and measurement noise, respectively. They are both independent zero mean Gaussian distribution with the known variance-covariance matrices $Q(k)$ and $R(k)$: $w(k) \sim N(0, Q(k))$ and $v(k) \sim N(0, R(k))$. The variance-covariance of the initial state $X(0|0)$ is expressed as $P(0|0)$. Assume that the estimate and variance–covariance at time k are denoted as $\hat{X}(k|k)$ and $P(k|k)$, respectively. The predicted estimate $\hat{X}(k+1|k)$ and the variance-covariance $P(k+1|k)$ at the time $k+1$ are:

$$\hat{X}(k+1|k) = f(k, \hat{X}(k|k))$$
$$P(k+1|k) = F(k, \hat{X}(k|k))P(k|k)F(k, \hat{X}(k|k))' + Q(k+1) \quad , (6)$$

where:

$$F(k, \hat{X}(k-1|k-1)) = \frac{\partial f(k, X(k))}{\partial X}\Big|_{X(k)=\hat{X}(k-1|k-1)} . \quad (7)$$

The predicting measurement value $Z(k+1|k)$ is:

$$Z(k+1|k) = h(k+1, \hat{X}(k+1|k)) \quad (8)$$

with its associated variance–covariance matrix and Kalman gain:

$$S(k+1) = H(k+1)P(k+1|k)H(k+1)' + R(k+1), \quad (9)$$

$$K(k+1) = (P(k+1|\text{k}))H(k+1)' \Big/ S(k+1), \quad (10)$$

where

$$H(k+1) = \frac{\partial h(X(k+1,k), k+1)}{\partial X(k+1)}\Big|_{X(k+1)=\hat{X}(k+1|k)} . \quad (11)$$

Updated state and variance–covariance are:

$$\hat{X}(k+1|k+1) = \hat{X}(k+1|k) + K(k+1)\left[Z(k+1) - Z(k+1|k)\right]$$
$$P(k+1|k+1) = \left[I - K(k+1)H(k+1, \hat{X}(k+1|k))\right]P(k+1|k) \quad , (12)$$

where I is the identity matrix.

III. TRACE OPTIMIZATION WITH NESTED PROBABILISTIC-NUMERICAL LINGUISTIC INFORMATION

The trace optimization process with the maneuvering target has limited and uncertain information. For example, the finite measurement information obtained using sensors or other detecting tools has systemic errors. These errors depend on various motion states that are unknown in advance for each instance of the maneuvering target. In this Section, we first employ data collecting and preprocessing and then optimize sensors' tracking errors at various motion states using nested probabilistic-numerical linguistic information. We then introduce the tracking optimization method based on EKF with nested probabilistic-numerical linguistic information (NPN-EKFTO) and propose the algorithm.

A. Notation

We first propose NPNLTSs based on PLTSs and other existing techniques. The parameters and notations are shown in Table I.

TABLE I
NOTATION

Notation	Description
S_k	k –th sensor, $k = 1, 2, \cdots, l$
J_i	i –th phases, $i = 1, 2, \cdots, m$
C_j	j –th evaluation index, $j = 1, 2, \cdots, n$
M_p	p –th motion state, $p = 1, 2, \cdots, q$
D^k	Distance between target and the k –th sensor
E_g	g –th expert system, $g = 1, 2, \cdots, t$
α	Azimuth angle
β	Pitch angle
T	Recording time
ω	Longitude
ϕ	Latitude
x^k, y^k, z^k	Three-dimensional coordinates of the maneuvering target in the sensor coordinate system
X^k, Y^k, Z^k	Three-dimensional coordinates of the sensor in the geocentric coordinate system
$\bar{X}^k, \bar{Y}^k, \bar{Z}^k$	Three-dimensional coordinates of the maneuvering target in the geocentric coordinate system

B. Unified coordinate system

During the tracking process, the sensors usually record spherical coordinate parameters such as the distance and azimuth and pitch angles. The measurement data are listed in Table II.

TABLE II
MEASUREMENT DATA USING SENSORS

Distance (m)	Azimuth angle (degree)	Pitch angle (degree)	Time (s)	Sensor label
D_1	α_1	β_1	T_1	S_1
D_2	α_2	β_2	T_2	S_2
D_3	α_3	β_3	T_3	S_3
…	…	…	…	…

The sensor measurements utilize their own coordinate system called sensor coordinate system (SCS). The SCS parameters are listed in Table III.

TABLE III
SCS PARAMETERS

Parameter	Description
Origin C	Sensor center
X-axis coordinate	Tangent between the sensor center C and the local latitude points to the East
Y-axis coordinate	Tangent between the sensor center C and the local longitude points to the North
Z-axis coordinate	Line between the earth's core and the sensor center C points to the sky
Azimuth angle α	Angle in the XY plane: range from 0 to 360 degrees
Pitch angle β	Angle between the sensor center and the CY-plane: range from -90 to 90 degrees

In Fig. 1, A and A' are the SCS position states at various positions of the maneuvering target. Shown also are the azimuth angle α and the pitch angle β.
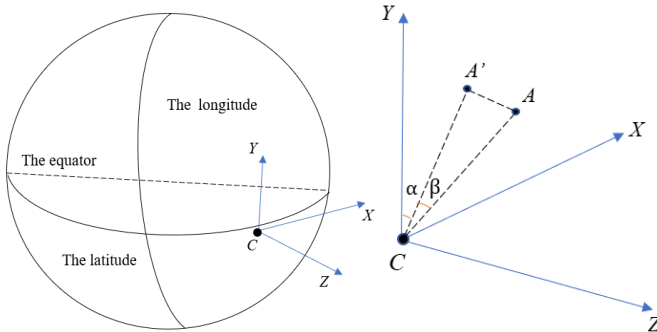

Fig. 1. The schematic SCS diagram using a sensor.

Multiple sensors are used to follow the maneuvering target in order to precisely detect the track. A sensor introduces a systemic error that cannot be avoided even though multiple sensors may reduce these errors. The position range of the maneuvering target may be narrowed by measuring data using multiple sensors at the same time instance. These sensors collect the measurement data during various periods using their independent sensor coordinate systems (SCSs). Since it is not convenient to observe the entire data collected at each time instance using multiple SCSs, we transform SCSs data to the geocentric coordinate system (GCS) shown in Fig. 2. GCS parameters are listed in Table IV.

TABLE IV
GCS PARAMETERS

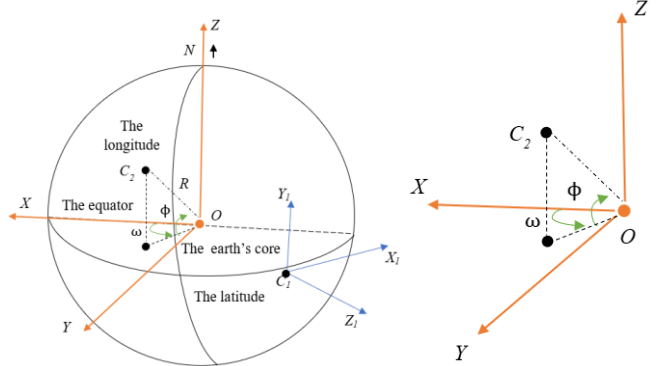| Parameter	Description
Origin O	Earth's core
X-axis coordinate	Intersection of the prime meridian plane and equatorial plane to the West
Y-axis coordinate	Right-handed system with the Y-axis and vertical XZ-plane
Z-axis coordinate	North overlaps with the rotation-axis of the Earth

Fig. 2. The GCS schematic diagram.

The GCS with the origin O and two SCSs with the sensor centers C_1 and C_2 are shown in Fig. 2. On the right, the GCS is expanded to illustrate transformation of SCSs to GCS. Let us assume that the GCS longitude and latitude coordinates of each sensor are $(\omega_k, \phi_k)(k = 1, 2, \cdots, l)$, where the range of the longitude ω_k is 0~180°W or 0~180°E and the range of the latitude ϕ_k is 0~90°N or 0~90°S. The radius of the Earth is R and the relative GCS position coordinates with the origins $C_k (k = 1, 2, \cdots, l)$ are:

$$X^k = R \times \cos(\omega_k / 180 \times \pi) \times \cos(\phi_k / 180 \times \pi)$$
$$Y^k = R \times \sin(\omega_k / 180 \times \pi) \times \cos(\phi_k / 180 \times \pi) \quad . \quad (13)$$
$$Z^k = R \times \sin(\phi_k / 180 \times \pi)$$

The translation and rotation transformation of coordinates between SCS and GCS leads to:

$$\begin{bmatrix} \bar{X}^k \\ \bar{Y}^k \\ \bar{Z}^k \end{bmatrix} = \begin{bmatrix} X^k \\ Y^k \\ Z^k \end{bmatrix} + L^k \begin{bmatrix} x^k \\ y^k \\ z^k \end{bmatrix}, \quad (14)$$

where $\left[\bar{X}^k, \bar{Y}^k, \bar{Z}^k \right]'$ are GCS coordinates of the maneuvering target, $\left[X^k, Y^k, Z^k \right]'$ are GCS coordinates of the sensor $S_k (k = 1, 2, \cdots, l)$, $\left[x^k, y^k, z^k \right]'$ are the SCS coordinates of the maneuvering target, and L^k is the transformation matrix between SCS and GCS.

Discussion: The range of the longitude ω is 0~180°W or 0~180°E. Hence, $\sin \omega$ has a significant positive or negative effect (13). Therefore, we consider two cases regarding the longitude ω:

(1) When the longitude $\omega \in (0,90^\circ]$, the sensor C_1 is located in 0~90°W or 0~90°E, as shown in Fig. 3.

In this case, $\sin \omega > 0$ and

$$\begin{aligned}
\bar{X} &= (-y\sin\phi + z\cos\phi)\cos\omega + x\sin\omega \\
\bar{Y} &= (-y\sin\phi + z\cos\phi)\sin\omega + x\cos\omega \\
\bar{Z} &= y\cos\phi + z\sin\phi
\end{aligned} \quad (15)$$

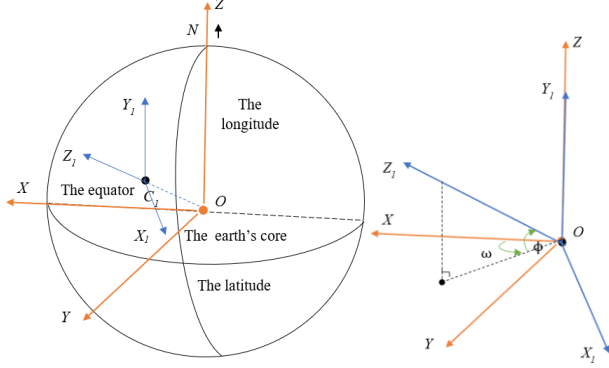Fig. 3. The GCS schematic diagram when the longitude $\omega \in (0,90^\circ]$.

(2) When the longitude $\omega \in (90^\circ, 180^\circ]$, the sensor C_2 is located in 90°W~180°W or 90°E~180°E, as shown in Fig. 4.
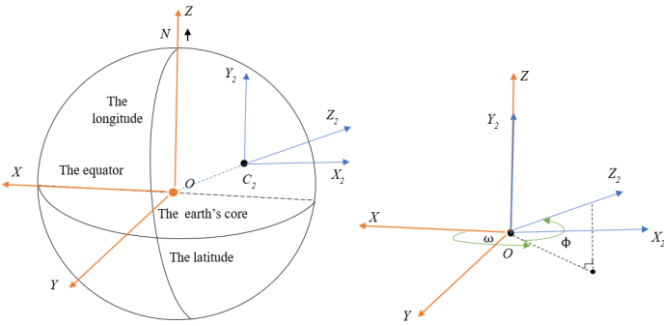

Fig. 4. The schematic diagram when the GCS longitude $\omega \in (90^\circ, 180^\circ]$.

In this case, $\sin \omega < 0$ and:

$$\begin{aligned}
\bar{X} &= (-y\sin\phi + z\cos\phi)\cos\omega - x\sin\omega \\
\bar{Y} &= (-y\sin\phi + z\cos\phi)\sin\omega + x\cos\omega \\
\bar{Z} &= y\cos\phi + z\sin\phi
\end{aligned} \quad (16)$$

C. Parameter optimization with nested probabilistic–numerical linguistic information

The measurement data recorded by different sensors contain errors in various motion states, where the motion state of the maneuvering target depends on the time instance. However, due to the uncertainty and complexity of the tracking errors, the systemic and maximum errors of the sensor at a certain motion state of the maneuvering target is often used to optimize the trace during the entire tracking process [5]. Therefore, it is necessary to minimize the tracking errors based on different motion states to further optimize tracking the maneuvering target. The maneuvering target often records motion states, such as constant velocity (CV), constant acceleration (CA), coordinate turn (CT), and current statistical (CS). We describe the maneuvering target at various phases during the tracking process using the nested probabilistic–numerical linguistic information.

Let $J = \{J_1, J_2, \cdots, J_m\}$ be a finite set of m phases during the tracking process and $C = \{C_1, C_2, \cdots, C_n\}$ be a set of n evaluation indexes with the weight vector $\omega = (\omega_1, \omega_2, \cdots, \omega_n)^T$, where $\omega_j \geq 0, j = 1,2,\cdots,n$ and $\sum_{i=1}^{n} \omega_i = 1$. Considering the evaluation indexes $C_j (j = 1,2,\cdots,n)$ over the phases $J_i (i = 1,2,\cdots,m)$, the expert systems evaluation information is represented by the OPLTSs $OL_{ij}(p) = \{OL_{ij}^{(h)}(p_{ij}^{(h)}) \mid h = 1,2,..., \#OL_{ij}(p)\}$, where $OL_{ij}^{(h)}(p_{ij}^{(h)})$ is the h–th linguistic term element in the OLTS $OS = \{s_\alpha \mid \alpha = 0,1,2,\cdots,\tau\}$ associated with the probability $p_{ij}^{(h)}$, $p_{ij}^{(h)} > 0$, and $\#OL_{ij}(p)$ is the number of linguistic term elements in $OL_{ij}(p)$. For example, suppose $OS = \{s_0 = CV, s_1 = CA, s_2 = CT, s_3 = CS\}$, when the expert systems consider that the motion state is s_1 over the phase J_i with respect to the evaluation index C_j with the sensor k, and its probability is 0.6. Then, the OPLTS is $OL_{ij}^k(p) = \{s_1(0.6)\}$. The outer–layer decision matrix $OR^k = \left[OL_{ij}^k(p) \right]_{m\times n}$ is shown in Table V.

TABLE V
THE OUTER–LAYER DECISION MATRIX OR^k

	C_1	C_2	⋯	C_n
J_1	$OL_{11}^k(p)$	$OL_{12}^k(p)$	⋯	$OL_{1n}^k(p)$
J_2	$OL_{21}^k(p)$	$OL_{22}^k(p)$		$OL_{2n}^k(p)$
⋮	⋮	⋮	⋱	⋮
J_m	$OL_{m1}^k(p)$	$OL_{m2}^k(p)$	⋯	$OL_{mn}^k(p)$

The second evaluation information over the outer-layer linguistic term elements $s_\alpha (\alpha = 0,1,\cdots,\tau)$ in the OLTS $OS = \{s_\alpha \mid \alpha = 0,1,2,\cdots,\tau\}$ with respect to the inner–layer linguistic term elements $n_\beta (\beta = 0,1,2,\cdots,\varsigma)$ in the ILTS $IS = \{n_\beta \mid \beta = 0,1,2,\cdots,\varsigma\}$ is represented by the INLTSs $IL_{\alpha\beta}(v) = \{IL_{\alpha\beta}^{(l)}(v_{\alpha\beta}^{(l)}) \mid l = 0,1,...,\varsigma\}$, where $IL_{\alpha\beta}^{(l)}(v_{\alpha\beta}^{(l)})$ is the l-th linguistic term in the ILTS associated with the value $v_{\alpha\beta}^{(l)}$, $v_{\alpha\beta}^{(l)} > 0$ and $\varsigma + 1$ is the number of inner-layer linguistic terms in $IL_{\alpha\beta}(v)$. For example, $IS = \{n_0 = distanse\,error, n_1 = azimuth\,angle\,error, n_2 = pitch\,angle\,error\}$, $s_1(0.6)$ with respect to the inner-layer linguistic term elements $n_\beta (\beta = 0,1,2)$ may be expressed as $s_1(0.6)\{n_0(50), n_1(5), n_2(10)\}$ indicating that the distance, the azimuth angle, and the pitch angle errors are 50, 5, and 10, respectively, under the motion state CA with probability 0.6. The inner-layer decision matrix $IR = \left[IL_{\alpha\beta}(v) \right]_{\tau\times\varsigma}$ is shown in Table VI.

TABLE VI
THE INNER–LAYER DECISION MATRIX IR

	n_0	n_1	$\cdots$	n_ς
s_0	$IL_{00}(v)$	$IL_{01}(v)$	$\cdots$	$IL_{0\varsigma}(v)$
s_1	$IL_{10}(v)$	$IL_{11}(v)$	$\vdots$	$IL_{1\varsigma}(v)$
$\vdots$	$\vdots$	$\vdots$	$\ddots$	$\vdots$
s_τ	$IL_{\tau 0}(v)$	$IL_{\tau 1}(v)$	$\cdots$	$IL_{\tau\varsigma}(v)$

Therefore, combined with the outer-layer decision matrix OR^k and the inner-layer decision matrix IR, the nested probabilistic-numerical linguistic decision matrix $R^k = \left[NPN^k \right]_{m\times n} = \left[\left\{ OL_{ij}^k(p)\left\{ IL_{\alpha\beta}(v)\right\}\right\}\right]_{m\times n}$ may be expressed using NPNLTSs as:

$$R^k = \left[NPN_{ij}^k \right]_{m\times n} = \begin{bmatrix} NPN_{11}^k & NPN_{12}^k & \cdots & NPN_{1n}^k \\ NPN_{21}^k & NPN_{22}^k & \cdots & NPN_{2n}^k \\ \vdots & \vdots & \ddots & \vdots \\ NPN_{m1}^k & NPN_{m2}^k & \cdots & NPN_{mn}^k \end{bmatrix}. \quad (17)$$

The overall decision matrix $R^k = \left[NPN_{ij}^k \right]_{m\times n}$ with the sensor k based on NPNLTSs is shown in Table VII.

TABLE VII
THE OVERALL DECISION MATRIX R^k

	C_1	C_2	$\cdots$	C_n
J_1	$OL_{11}^k(p)\{IL(v)\}$	$OL_{12}^k(p)\{IL(v)\}$	$\cdots$	$OL_{1n}^k(p)\{IL(v)\}$
J_2	$OL_{21}^k(p)\{IL(v)\}$	$OL_{22}^k(p)\{IL(v)\}$		$OL_{2n}^k(p)\{IL(v)\}$
$\vdots$	$\vdots$	$\vdots$	$\ddots$	$\vdots$
J_m	$OL_{m1}^k(p)\{IL(v)\}$	$OL_{m2}^k(p)\{IL(v)\}$	$\cdots$	$OL_{mn}^k(p)\{IL(v)\}$

Finally, we may aggregate $R^k = \left[NPN_{ij}^k \right]_{m\times n}$ from the OPLTSs and the INLTSs to get the optimized error parameters $IZ_i = \left\{ n_\beta\left(v_i^* \right)\right\}$ over the phase J_i. If the inner linguistic term set of the error parameters is $IS = \left\{ n_0 = D, n_1 = \alpha, n_2 = \beta \right\}$, the optimized error parameters $\left(D_{op}^i, \alpha_{op}^i, \beta_{op}^i \right)$ may be obtained considering the overall factors such as the sensor type, motion state, and state phases.

D. Trace optimization

Due to the complex environment of the maneuvering target, the state estimation system is nonlinear. Combined with the EKF, f and h (5) are both nonlinear functions. Let $\tilde{X} = X(k-1) - (k-1)$ and $\hat{X} = X(k) - \hat{k}$. Linearization using Taylor series and taking EKF as the first-order gives:

$$f\left(k, X(k-1) \right) \approx f(k, k-1) + f'(k, k-1)\left(\tilde{X} \right) \underset{f'(k,k-1)=:G_k}{=} f(k, k-1) + G_k\left(\tilde{X} \right), \quad (18)$$

$$h\left(k, X(k) \right) \approx h\left(\hat{k} \right) + h'\left(\hat{k} \right)\left(\hat{X} \right) \overset{h'(k)=:H_k}{=} h\left(\hat{k} \right) + H_k\left(\hat{X} \right). \quad (19)$$

We next insert relevant parameters: the initial state $X(0|0)$, the observation vector $Z(k)$, the process noise $w(k)$, the

measurement noise $v(k)$, and the initial variance–covariance $P(0|0)$. In particular, the variance–covariance at time k (6) depends on the optimized error parameters calculated in Section III-C.

We finally calculate the predicted measurement value $Z(k+1|k)$ (8) with its associated variance–covariance matrix $S(k+1)$ (9) and the Kalman gain $K(k+1)$ (10) to further update the state $\hat{X}(k+1|k+1)$ and the variance–covariance $P(k+1|k+1)$ (12). We then obtain the optimized tracking based on nested probabilistic–numerical linguistic information.

E. NPN-EKFTO: Algorithm

The main steps of the tracking optimization algorithm using the NPN–EKFTO method are:

Step 1. Collect the spherical coordinate parameters from the sensors and transform them to the three–dimensional coordinate parameters of the maneuvering target.

Step 2. Convert each SCS to the GCS and describe the scatter diagram and initial GCS trajectory of the maneuvering target.

Step 3. Optimize the coordinates by the data preprocessing (having at least two recording data points at the same time instance) and divide the movement phases of the maneuvering target according to the initial trajectory.

Step 4. Given the NPNLTSs by expert systems about the error parameters over various phases at various motion states with respect to the evaluation indexes, aggregate NPNLTSs to obtain the optimized error parameters at each phase.

Step 5. Obtain the optimal tracking with optimized error parameters based on the EKF algorithm.

The tracking optimization process based on the NPN–EKFTO method is implemented in the NPN-EKFTO Algorithm:

Algorithm: NPN-EKFTO

Input parameters:

P – the number of processes L – the number of sensors

M – the number of phrases T_i – the recording time of process i

D_i^k – the distance with sensor k of process i

α_i^k – the azimuth angle with sensor k of process i

β_i^k –the pitch angle with sensor k of process i

1. *// Calculate coordinates in GCS*

2. for i : =1 to P

3.   for k : =1 to L

4. $[X_i^k, Y_i^k, Z_i^k] := GCS[D_i^k, \alpha_i^k, \beta_i^k]$

5.   loc $(T_i) := [X_i, Y_i, Z_i]$

6. *// Select repetition time*

7. i = 1, ii=1

8. while (i ~ = P+1)

9.   if number $(T_i) >1$

10.   i=i+1

11.   if length (number $(T_i)) \sim = 1$

12.   ii=ii+1, i=i+1

13.   repetition time : = T_i +1

14. *// Do data preprocessing*

15.   if ii ~ = 1

16.   location (T_i) : = overlapping region (repetition time)

17.   else
18.   return location (T_i)
19.   // Optimize the error parameters
20.   for i = 1 to P
21.   for j = 1 to M
22.   [D_{op}^i , α_{op}^i , β_{op}^i] : = aggregate. NPN [D_{ij} , α_{ij} , β_{ij}]
23.   // Optimize tracking based on EKF
24.   for i = 2 to P
25.   predict. loc (i) : = f_nonlinear (optimal. loc (i), optimal. loc (i-1))
26.   predict. cov (i) : = cov (i-1) + R. cov (i)
27.   gain (i) : = predict. cov (i) * (predict. cov (i) + Q. cov (i)) $^{-1}$
28.   optimal. loc (i) : = predict. loc (i) + gain (i) * coefficient (i)
29.   cov (i) : = (I - gain (i)) * predict. cov (i)
30.   return optimal. loc (i)
31.   return cov (i)

F. NPN-EKFTO: Flow chart

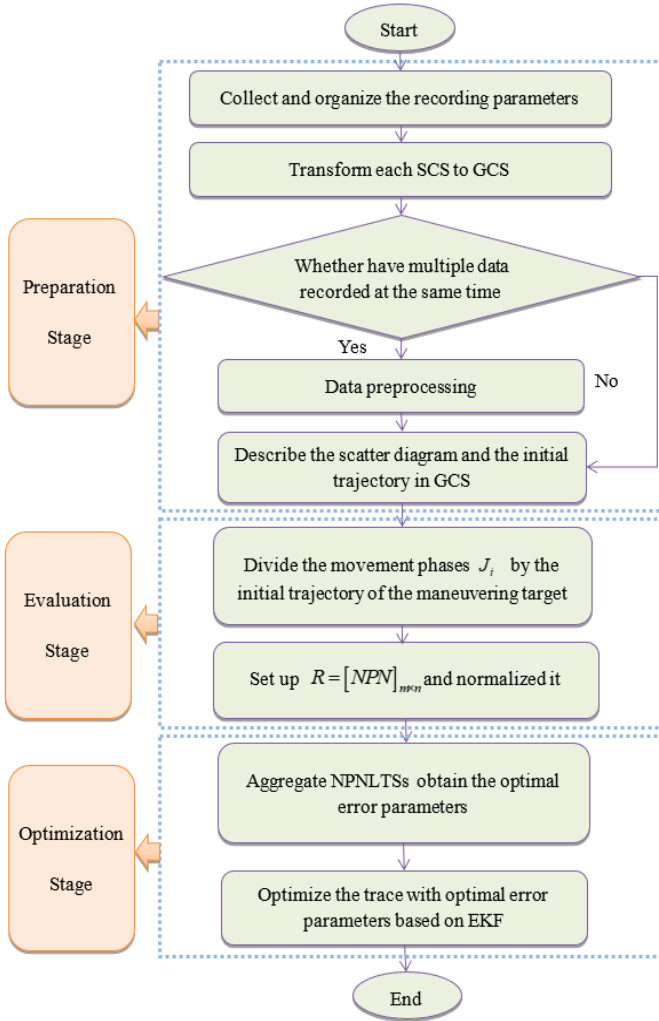The flow chart of the NPN-EKFTO algorithm is shown in Fig. 5.

Fig. 5. The flow chart of the NPN-EKFTO algorithm.

The NPN-EKFTO system may be divided into three stages: The preparation stage that transforms each SCS coordinate to GCS and organizes the recording parameters in the three–dimensional GCS coordinates; The evaluation stage that assesses the tracking error parameters over different phases at various motion states with respect to the evaluation NPNLTSs indexes; The tracking of the maneuvering target with the optimal error parameters based on the EKF algorithm.

IV. CASE STUDY OF THE MANEUVERING TARGET TRACKING USING THE NPN-EKFTO METHOD

A. Case description

Target tracking is very important in predicting the intentions of the maneuvering target in many fields. Maneuvering target tracking technology is indispensable in securing personal safety, financial security, and information assurance.

We consider the case of an unknown maneuvering target in Sichuan province. Sichuan province, located in Southwestern China, is topographically high in the West and low in the East. It is well-known for its complex terrain with plains, hills, mountains, and plateaus, offering rich environmental factors for target tracking. In order to detect the maneuvering target's intent and guide its action, the instructor requires tracking the status of the maneuvering target using three sensors. The tracking data are returned from real-world experiments in real time. 728 sets of measurement data of the maneuvering target are collected with the three sensors at slightly different times. Specifically, sensor 1, sensor 2, and sensor 3 record 237, 264, and 227 sets of measurement data, respectively. The measurement data (partial list) and the correlation system information from the three sensors are shown in Table VIII and Table IX, respectively.

TABLE VIII
PART LIST OF THE MEASUREMENT DATA USING THREE SENSORS

Distance (m)	Azimuth angle (degree)	Pitch angle (degree)	Time (s)	Sensor label
61709.26	29.03	0.28	36620.4	1
61566.09	29.30	0.18	36621.4	1
61556.81	30.01	0.39	36622.4	1
…	…	…	…	…
65030.10	32.76	0.30	36874.4	1
56774.49	173.61	0.12	36919.4	2
56861.94	173.89	0.02	36920.4	2
56846.59	174.22	0.64	36921.4	2
…	…	…	…	…
63469.37	173.71	0.29	37119.4	2
18367.97	280.84	1.67	37119.4	3
63348.41	173.53	0.12	37120.4	2
18346.51	281.78	2.04	37120.4	3
…	…	…	…	…
21310.12	281.00	1.54	37367.4	3
21069.02	280.54	1.69	37368.4	3
21143.01	281.39	1.84	37369.4	3

Remark 1. Sensor 1 records the measurement data of the maneuvering target at different times. There are no identical recording times using Sensor 2 and Sensor 3. Sensor 2 and Sensor 3 have 79 identical recording times.

TABLE IX
THE CORRELATION SYSTEM INFORMATION USING THREE SENSORS

Sensor label	Longitude ω (degree)	Latitude ϕ (degree)	Height h (m)
1	102.1	30.5	0
2	102.4	31.5	0
3	102.7	31.9	0

Remark 2. The three sensors are located in the horizontal plane, as evident by their heights. They are located at the East longitudes and the North latitudes.

Based on the longitudes of the three sensors shown in Table VIII, $\omega^k \in \left(90°, 180°\right]$ $\left(k = 1, 2, 3\right)$ and, hence, belong to the second phase described in Section III-B. Thus, we may construct the transformation matrix L^k as:

$$L^k = \begin{bmatrix} -\sin\omega^k & -\sin\phi^k\cos\omega^k & \cos\phi^k\cos\omega^k \\ \cos\omega^k & -\sin\phi^k\sin\omega^k & \cos\phi^k\sin\omega^k \\ 0 & \cos\phi^k & \sin\phi^k \end{bmatrix}.$$

Combined with (14), we have:

$$\begin{bmatrix} \bar{X}^k \\ \bar{Y}^k \\ \bar{Z}^k \end{bmatrix} = \begin{bmatrix} X^k \\ Y^k \\ Z^k \end{bmatrix} + \begin{bmatrix} -\sin\omega^k & -\sin\phi^k\cos\omega^k & \cos\phi^k\cos\omega^k \\ \cos\omega^k & -\sin\phi^k\sin\omega^k & \cos\phi^k\sin\omega^k \\ 0 & \cos\phi^k & \sin\phi^k \end{bmatrix} \begin{bmatrix} x^k \\ y^k \\ z^k \end{bmatrix}.$$

Therefore, relative GCS coordinates $\left[\bar{X}^k, \bar{Y}^k, \bar{Z}^k\right]$ $\left(k = 1, 2, 3\right)$ of the maneuvering target may be obtained from the SCS. Trajectories of the maneuvering target in three SCSs and the GCS are shown as track diagrams in Fig. 6.

Figures 6 (a) to (c) show that the shape of the track diagram using Sensor 1 is similar to a "U" shape while the shapes of the track diagrams using Sensor 2 and Sensor 3 both have spiral shapes. The overall track of the maneuvering target using three sensors, shown in Fig. 6(d), is similar to the position coordinates using Sensor 2 and Sensor 3 while the track diagram using Sensor 1 is relatively independent. This observation corresponds to Remark 1.
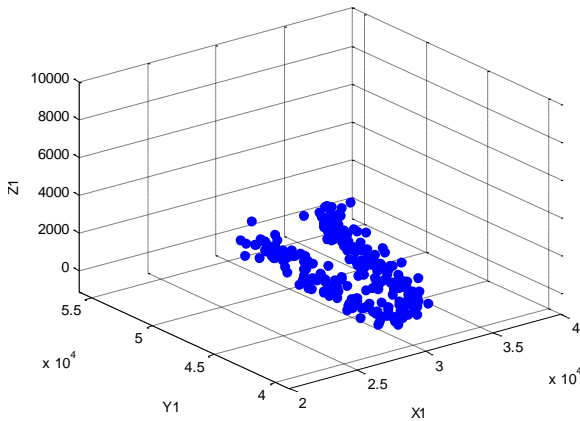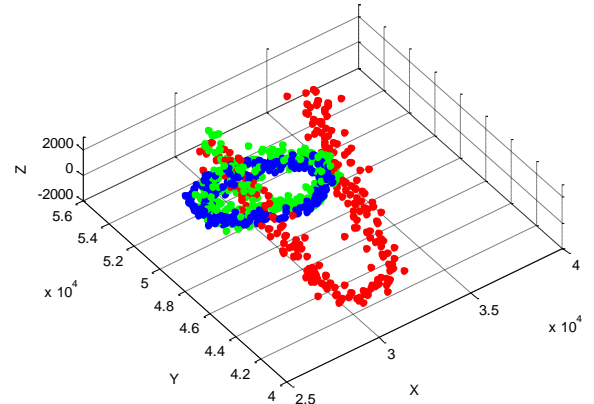

(a) SCS$_1$: Track diagram
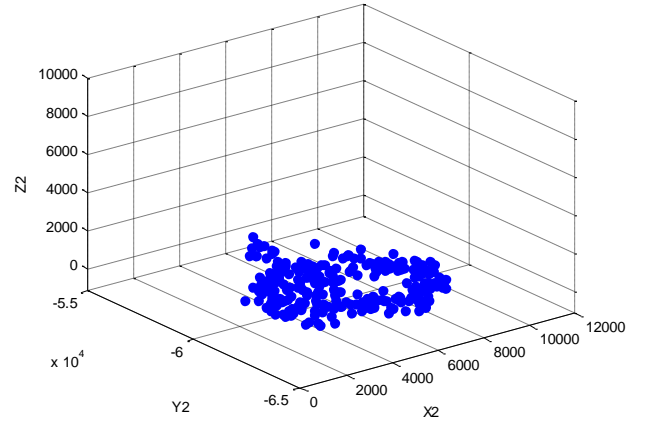
(b) SCS$_2$: Track diagram.
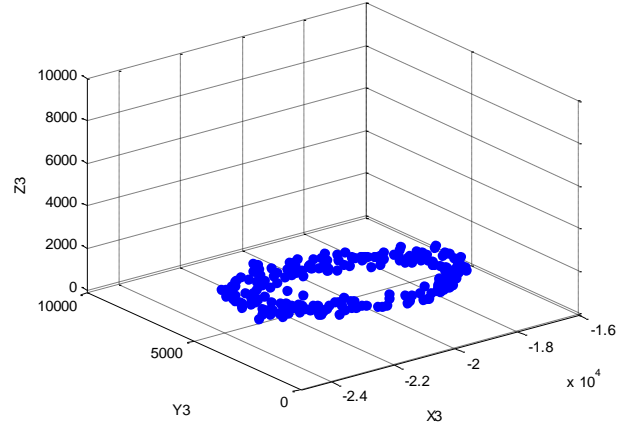
(c) SCS$_3$: Track diagram in.

(d) GCS: Track diagrams.

Fig. 6. Track diagrams of the maneuvering target in SCSs and GCS.

B. Data preprocessing

The location parameters of a maneuvering target such as the longitude, the latitude, and the height should be unique at each time instance [44]. However, according to Table VIII and Remark 1, the recording times are not unique when the three sensors track the maneuvering target because measurement data are recorded at the same time instance by different sensors. Therefore, it is necessary to narrow the range of possible positions of the maneuvering target at each moment using the systemic error parameters (data preprocessing) and then further

optimize its track. Examples of systemic error parameters for the three sensors are shown in Table X.

TABLE X
SYSTEMIC ERROR PARAMETERS FOR THE THREE SENSORS

Sensor label	Distance–measuring error D (m)	Error of α (degree)	Error of β (degree)
1	50	0.4	0.4
2	60	0.5	0.5
3	60	0.5	0.5

Remark 3. The sensors' systemic error parameters when measuring the distance D, the azimuth angle α, and the pitch angle β shown in Table VIII are the maximum errors considering multiple factors in as many cases as possible during the tracking process.

According to the measurement data, Sensor 2 and Sensor 3 have the same recording times during the time interval 37,119.4 s to 37,219.4 s where there are 79 sets of overlapping measurement data at the same time instance. For example, in 494th and 495th sets of the measurement data, the relevant position parameters with Sensor 2 and Sensor 3 are shown in Table XI.

TABLE XI
POSITION PARAMETERS AT 494TH AND 495TH SETS

Sensor label	Distance (m)	Azimuth angle (degree)	Pitch angle (degree)	Time (s)
2	60,583	174.3312	0.1283	37,164
3	19,997	289.3387	0.9417	37,164

According to the systemic error parameters shown in Table VIII, we may identify possible positions and the overlapping region at 494th and 495th sets with Sensor 2 and Sensor 3 as shown in Fig. 7.
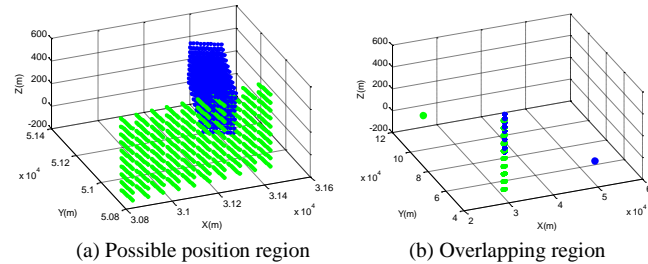

(a) Possible position region   (b) Overlapping region
Fig. 7. Possible position and overlapping regions at 494th and 495th sets.

Fig. 7 (a) represents possible position regions at 494th and 495th sets with Sensor 2 and Sensor 3 at the same time instance: the green area shows possible position region at 494th under the systemic errors with the Sensor 2 while the blue area shows possible position region at 495th under the systemic errors with Sensor 3. Fig. 7(b) shows the overlapping region between the green and the blue areas. The most likely position at this time instant should be in the overlapping region because it satisfies both systemic errors with both sensors. Hence, the range of the possible position region of the maneuvering target can be narrowed down by data preprocessing, as shown in Fig. 7. Therefore, the position accuracy of tracking the maneuvering

target will be greatly improved by considering all 79 sets of overlapping measurement data.

C. Using the NPN-EKFTO method

Based on the NPN-EKFTO algorithm introduced in Section III-E, the initial trajectory of the maneuvering target needs to be described by considering various movement phases. After data preprocessing described in Section IV-B, we may generate the observable trace with the maneuvering target shown in Fig. 8.
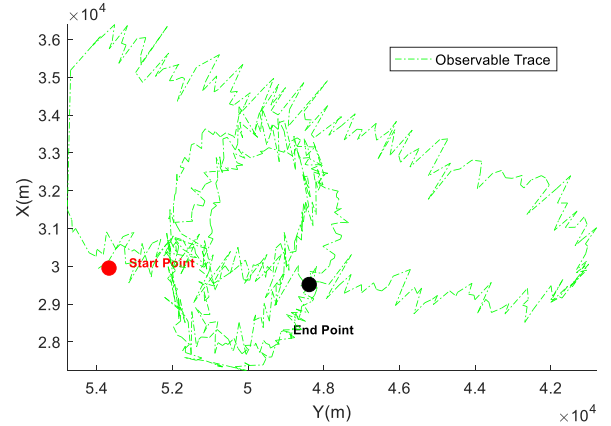
(a) Observable trace.
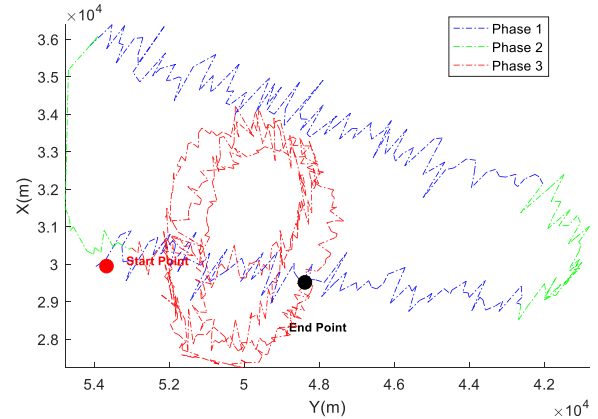
(b) Movement phases.

Fig. 8. The initial trajectory of the maneuvering target.

Remark 4. Three main phases of motion states need to be evaluated from the start to end point shown in Fig. 8 (a). Note that Phase 1 (blue track) is similar to a straight-line movement, Phase 2 (green track) is similar to a turning motion, and Phase 3 (red track) resembles circular movement, as shown in Fig. 8 (b).

NPNLTSs are then used to optimize the error parameters with respect to various motion states of the corresponding phases and analyze the trace optimization by taking into account three main evaluation indexes: (1) C_1: movement shape; (2) C_2: accelerated speed; and (3) C_3: location coordinate. The weight vector is $\omega = (0.3, 0.5, 0.2)^T$. We define the OLTS and ILTS:

$$OS = \{s_0 = CV, s_1 = CA, s_2 = CT, s_3 = CS\}$$

$IS = \{n_0 = distance\ error, n_1 = azimuth\ angle\ error, n_2 = pitch\ angle\ error\}$.

In order to evaluate phases $J_i (i = 1, 2, 3)$, where the elements of OLTS are types of motion state introduced in Section III-C while the elements of ILTS are error parameters. Combined with the systemic error parameters using sensors shown in Table VIII, the inner–layer information matrices of the error parameters with respect to various motion states with different sensors is shown in Table XII.

Table XII
INNER–LAYER INFORMATION MATRIX USING DIFFERENT SENSORS

Sensor 1	n_0	n_1	n_2
s_0	40	0.3	0.3
s_1	30	0.2	0.2
s_2	50	0.4	0.4
s_3	40	0.3	0.3
Sensor 2	n_0	n_1	n_2
s_0	50	0.4	0.4
s_1	40	0.3	0.3
s_2	60	0.5	0.5
s_3	50	0.4	0.4
Sensor 3	n_0	n_1	n_2
s_0	50	0.4	0.4
s_1	40	0.3	0.3
s_2	60	0.5	0.5
s_3	50	0.4	0.4

The outer-layer information about the motion states with respect to evaluation indexes at different phases may be given as probabilities by expert systems, as shown in Table XIII. After collecting the outer-layer and the inner-layer information related to three sensors, we obtain the overall information matrix $R = \left[NPN_{ij} \right]_{m \times n}$ with nested probabilistic–numerical linguistic information.

TABLE XIII
THE OVERALL INFORMATION MATRIX R

	C_1	C_2	C_3
J_1	$\begin{Bmatrix} s_0(0.6)\{n_0(40),n_1(0.3),n_2(0.3)\}, \\ s_1(0.4)\{n_0(30),n_1(0.2),n_2(0.2)\}, \\ s_2(0)\{n_0(50),n_1(0.4),n_2(0.4)\}, \\ s_3(0)\{n_0(40),n_1(0.3),n_2(0.3)\}, \end{Bmatrix}$	$\begin{Bmatrix} s_0(0.6)\{n_0(40),n_1(0.3),n_2(0.3)\}, \\ s_1(0.3)\{n_0(30),n_1(0.2),n_2(0.2)\}, \\ s_2(0)\{n_0(50),n_1(0.4),n_2(0.4)\}, \\ s_3(0.1)\{n_0(40),n_1(0.3),n_2(0.3)\}, \end{Bmatrix}$	$\begin{Bmatrix} s_0(0.5)\{n_0(40),n_1(0.3),n_2(0.3)\}, \\ s_1(0.5)\{n_0(30),n_1(0.2),n_2(0.2)\}, \\ s_2(0)\{n_0(50),n_1(0.4),n_2(0.4)\}, \\ s_3(0)\{n_0(40),n_1(0.3),n_2(0.3)\}, \end{Bmatrix}$
J_2	$\begin{Bmatrix} s_0(0)\{n_0(40),n_1(0.3),n_2(0.3)\}, \\ s_1(0)\{n_0(30),n_1(0.2),n_2(0.2)\}, \\ s_2(0.7)\{n_0(50),n_1(0.4),n_2(0.4)\}, \\ s_3(0.3)\{n_0(40),n_1(0.3),n_2(0.3)\}, \end{Bmatrix}$	$\begin{Bmatrix} s_0(0)\{n_0(40),n_1(0.3),n_2(0.3)\}, \\ s_1(0)\{n_0(30),n_1(0.2),n_2(0.2)\}, \\ s_2(0.8)\{n_0(50),n_1(0.4),n_2(0.4)\}, \\ s_3(0.2)\{n_0(40),n_1(0.3),n_2(0.3)\}, \end{Bmatrix}$	$\begin{Bmatrix} s_0(0.1)\{n_0(40),n_1(0.3),n_2(0.3)\}, \\ s_1(0)\{n_0(30),n_1(0.2),n_2(0.2)\}, \\ s_2(0.7)\{n_0(50),n_1(0.4),n_2(0.4)\}, \\ s_3(0.2)\{n_0(40),n_1(0.3),n_2(0.3)\}, \end{Bmatrix}$
J_3	$\begin{Bmatrix} s_0(0.1)\{n_0(50),n_1(0.4),n_2(0.4)\}, \\ s_1(0.1)\{n_0(40),n_1(0.3),n_2(0.3)\}, \\ s_2(0.3)\{n_0(60),n_1(0.5),n_2(0.5)\}, \\ s_3(0.5)\{n_0(50),n_1(0.4),n_2(0.4)\} \end{Bmatrix}$	$\begin{Bmatrix} s_0(0.1)\{n_0(50),n_1(0.4),n_2(0.4)\}, \\ s_1(0.1)\{n_0(40),n_1(0.3),n_2(0.3)\}, \\ s_2(0.2)\{n_0(60),n_1(0.5),n_2(0.5)\}, \\ s_3(0.6)\{n_0(50),n_1(0.4),n_2(0.4)\} \end{Bmatrix}$	$\begin{Bmatrix} s_0(0.2)\{n_0(50),n_1(0.4),n_2(0.4)\}, \\ s_1(0.1)\{n_0(40),n_1(0.3),n_2(0.3)\}, \\ s_2(0.3)\{n_0(60),n_1(0.5),n_2(0.5)\}, \\ s_3(0.4)\{n_0(50),n_1(0.4),n_2(0.4)\} \end{Bmatrix}$

Remark 5. Although the error parameters using the sensor vary under different motion states, they should all be smaller than the systemic maximum errors using the corresponding sensors

shown in Table VIII. Furthermore, it can be seen that Sensor 1 traces Phase 1 and Phase 2, while the measurement data of Phase 3 should come from Sensor 2 and Sensor 3 shown in Fig. 6 and Fig. 8, respectively. Because the error parameters are identical using Sensor 2 and Senor 3 shown in Table VIII and Table X, respectively, there is no difference in errors between Sensor 2 and Sensor 3.

We now need to aggregate the NPNLTs shown in Table XI based on the method introduced in Section II-A and obtain the optimized error parameters at each phase. The outer-layer results $OZ_i(\omega)(i = 1, 2, 3)$ are:

$$OZ_1(\omega) = \{s_0(0.58), s_1(0.37), s_2(0), s_3(0.05)\}$$
$$OZ_2(\omega) = \{s_0(0.02), s_1(0), s_2(0.75), s_3(0.23)\}$$
$$OZ_3(\omega) = \{s_0(0.12), s_1(0.1), s_2(0.25), s_3(0.53)\}$$

The outer–layer's scores $OE(OZ_i(\omega)) (i = 1, 2, 3)$ are:

$$OE(OZ_1(\omega)) = s_{0.52}, OE(OZ_2(\omega)) = s_{2.19}, OE(OZ_3(\omega)) = s_{2.19}.$$

Thus, the inner–weight vector can be obtained as:

$$\varepsilon_1 = (0, 0.48, 0.52, 0)^T, \varepsilon_2 = (0, 0, 0.81, 0.19)^T, \varepsilon_3 = (0, 0, 0.81, 0.19)^T.$$

Finally, we optimize and aggregate the INLTSs with the inner–weight:

$$IZ_1(\varepsilon_1) = \{n_0(40.4), n_1(0.304), n_2(0.304)\}$$
$$IZ_2(\varepsilon_2) = \{n_0(48.1), n_1(0.381), n_2(0.381)\}.$$
$$IZ_3(\varepsilon_3) = \{n_0(58.1), n_1(0.481), n_2(0.481)\}$$

Thus, the optimal error parameters $\left(D_{op}^i, \alpha_{op}^i, \beta_{op}^i \right)$ with respect to the phases $J_i (i = 1, 2, 3)$ are $\left(D_{op}^1, \alpha_{op}^1, \beta_{op}^1 \right) = (40.4, 0.304, 0.304)$, $\left(D_{op}^2, \alpha_{op}^2, \beta_{op}^2 \right) = (48.1, 0.381, 0.381)$, and $\left(D_{op}^3, \alpha_{op}^3, \beta_{op}^3 \right) = (58.1, 0.481, 0.481)$, respectively. Then, the optimal tracking of the maneuvering target may be described based on the EKF algorithm with the optimal error parameters, as shown in Fig. 9.

The entire trace of the maneuvering target is shown in Fig. 9, where the red and black dots are the start and end points, respectively. The green and blue dashed lines are the observation and the filtered traces, respectively.

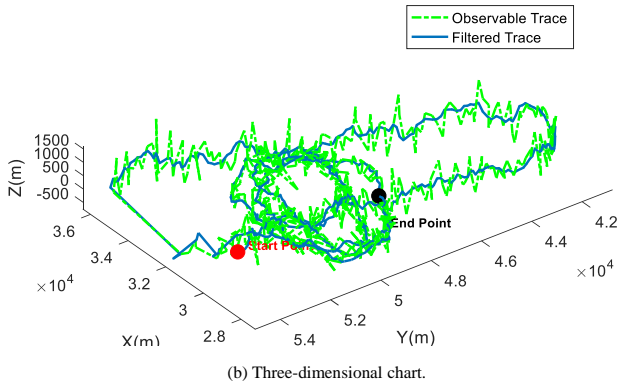(a) Two-dimensional chart.

(b) Three-dimensional chart.
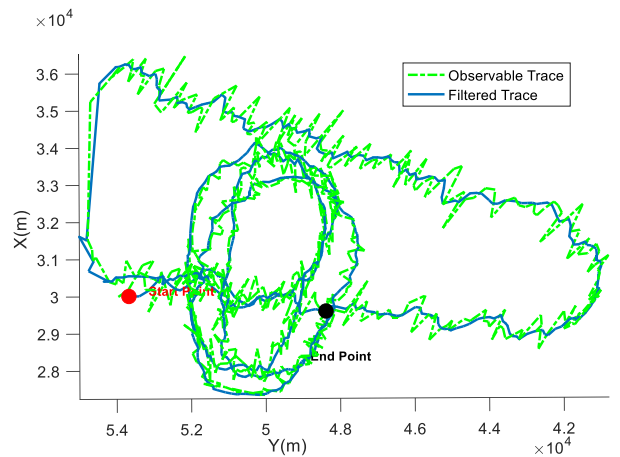
Fig. 9. The optimal tracking of the maneuvering target.

After transforming the coordinate system from SCSs to GCS and after data preprocessing, we obtain the optimized error parameters of the three sensors at each phase and then get the optimal tracking of the maneuvering target based on the NPN-EKFTO approach. As shown in Fig. 9, the tracking of the maneuvering target is similar to cruising first over a wide range and then reduces to a circle around a certain area. Therefore, we may focus on this area to deduce the intention of the maneuvering target. The proposed method enables us to define the area more precisely through the optimal tracking.

V. COMPARATIVE ANALYSES

In order to show the advantages of the proposed method, we consider effect of using multiple sensors, the EKF algorithm, and NPN linguistic information.

A. Multiple sensors

When tracking a maneuvering target by a sensor, the measurement data at a time is unique. The filtered trace only depends on the data and the sensor's error. However, multiple sensors may reduce the detection error of the target as discussed in Section IV-B. In the case study, there are 79 sets of overlapping measurement data by Sensor 2 and Sensor 3 at the same time instance. According to the observable points, we obtain filtered traces using one sensor and two sensors. The performances are shown in Fig. 10.

(a) Filtered trace by one sensor.   (b) Filtered trace by two sensors.
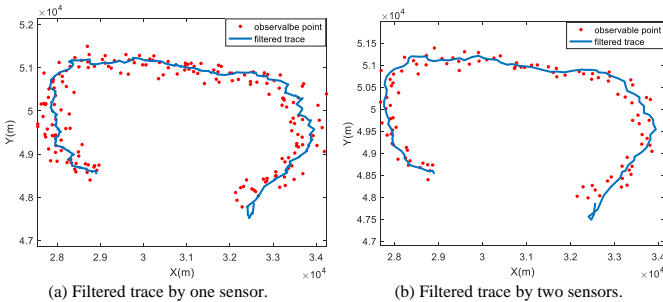
Fig. 10. Observable points and the filtered trace of the maneuvering target.

Within the same time frame, the data points are more dispersed in Fig. 10 (a) than in Fig. 10 (b). After data preprocessing, the filtered trace is much smoother than when using a single sensor. We next compare the observable trace and the filtered trace using EKF with one and two sensors, respectively.

(a) Filtered trace by one sensor.
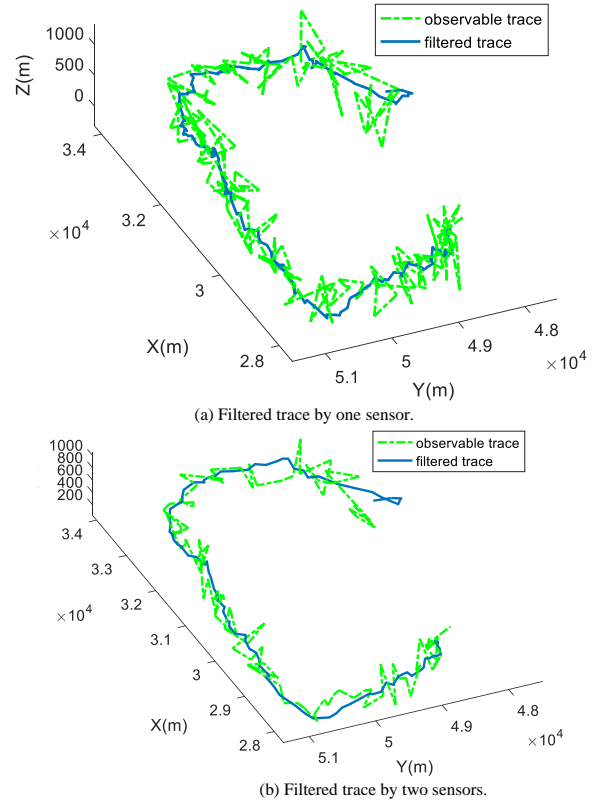

(b) Filtered trace by two sensors.

Fig. 11. The observable trace and filtered trace of the maneuvering target.

The observable trace using one sensor shown in Fig. 11(a) fluctuates more widely than using two sensors. The filtered trace based on EKF is much smoother, as shown in Fig. 11 (b).

Furthermore, the errors in X, Y, and Z derived by using different numbers of the sensors are shown in Fig. 12, Fig. 13, and Fig. 14, respectively.

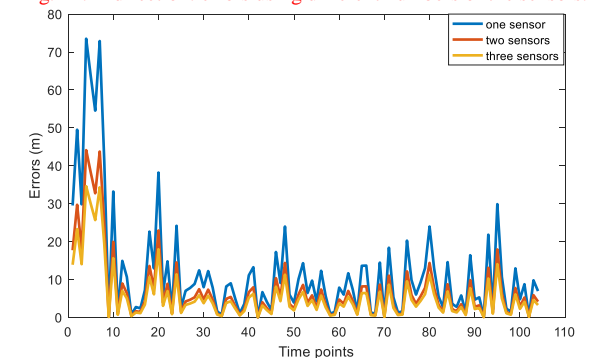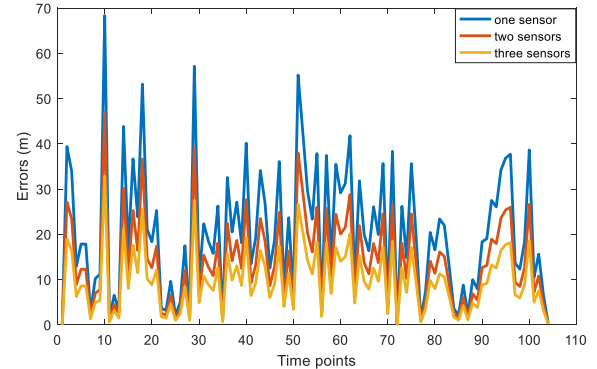Fig. 12. X direction: errors using different numbers of the sensors.

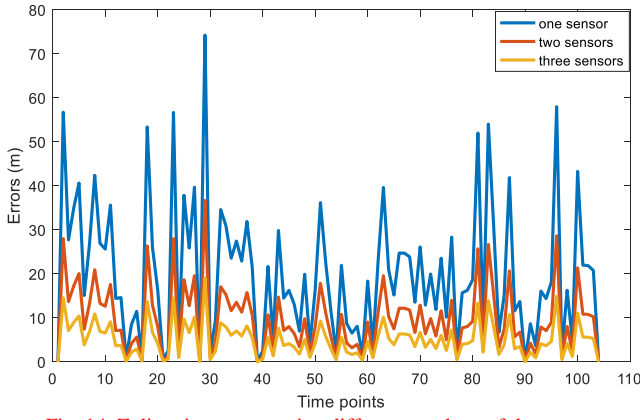Fig. 13. Y direction: errors using different numbers of the sensors.

Fig. 14. Z direction: errors using different numbers of the sensors.

As expected, the errors when using three sensors are the smallest than those in other two situations. The performances are also evaluated when using different numbers of the sensors, and when using different combinations of the sensors. Parameters such as mean error (ME), mean-square error (MSE), and standard deviation (SD) are shown in Table XIV, and in Table XV, respectively.

Table XIV
COMPARISONS OF ERRORS USING DIFFERENT NUMBERS OF SENSORS

X direction	ME	MSE	SD
One sensor	15.6924	75.7635	9.4324
Two sensors	9.5373	46.7834	4.7534
Three sensors	7.4159	32.7825	3.6713
Y direction	ME	MSE	SD
One sensor	10.2747	57.3245	8.5642
Two sensors	6.5635	36.7832	5.0636
Three sensors	4.7931	33.5591	4.1074
Z direction	ME	MSE	SD
One sensor	19.5393	96.3462	15.4687
Two sensors	10.4535	68.2144	8.6206
Three sensors	8.4913	58.2351	6.8924

Table XV
COMPARISONS OF ERRORS USING DIFFERENT COMBINATIONS OF SENSORS

X direction	ME	MSE	SD
Sensor 1 and Sensor 2	9.1417	45.9653	4.7856
Sensor 1 and Sensor 3	9.2565	46.0164	4.8215
Sensor 2 and Sensor 3	11.6746	48.9042	5.6543
Y direction	ME	MSE	SD
Sensor 1 and Sensor 2	6.7881	37.5427	5.6724
Sensor 1 and Sensor 3	6.8932	37.9752	5.8924
Sensor 2 and Sensor 3	8.2351	39.2409	6.9982
Z direction	ME	MSE	SD
Sensor 1 and Sensor 2	10.3852	68.9924	8.5785
Sensor 1 and Sensor 3	11.0324	70.1954	9.1241
Sensor 2 and Sensor 3	13.5362	72.3499	11.2733

According to statistical values shown in Table XIV and Table XV, errors with three sensors are the smallest ones. When using different combinations of sensors, the performances depend on the systematic errors of the sensor. For example, there are little difference of errors when using the sensor 1 and the sensor 2 or 3 because of the same systematic errors of the sensor 2 and the sensor 3. Hence, since multiple sensors effectively reduce errors based on data preprocessing, tracking a maneuvering target by multiple sensors is more accurate.

B. EKF algorithm

In addition to the EKF algorithm, there are other filtering algorithms that deal with nonlinear systems, such as the UKF and the CKF. In order to verify the proposed method, we recorded 1,200 sets of data using three sensors. There are 400 sets of overlapping measurement data at the same time instance. We conduct the case study using EKF, UKF, and CKF methods. The errors in X, Y, and Z directions are shown in Fig. 15, Fig. 16, and Fig. 17, respectively.
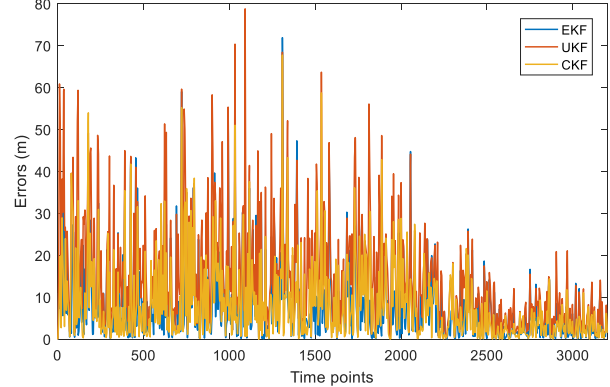

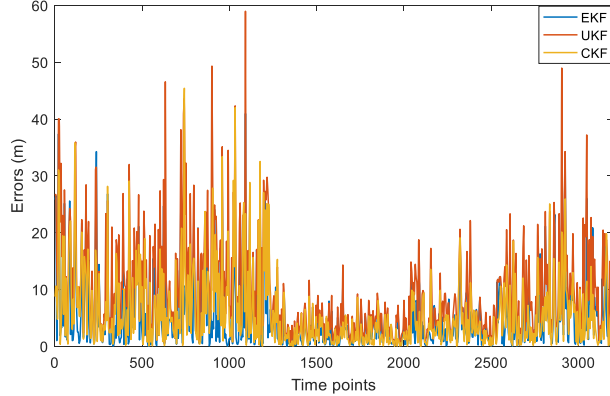Fig. 15. Errors in the X direction.
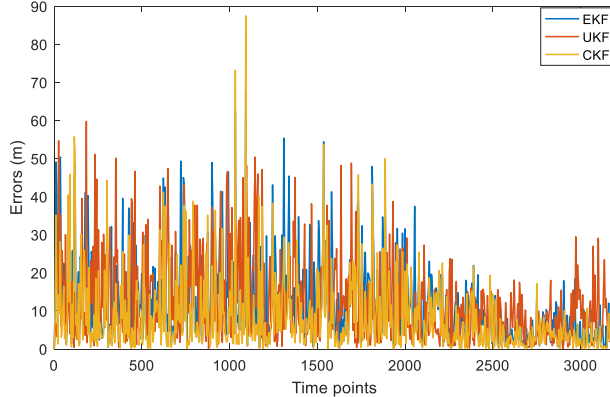

Fig. 16. Errors in the Y direction.

Fig. 17. Errors in the Z direction.

Fig. 15 to Fig. 17 show the errors in X, Y, and Z directions when using three different filtering algorithms. The direction in which the greatest average error is in the Z direction, and the smallest average error is in the Y direction. The errors are smaller by using the EKF than those by using UKF and CKF.

Since performance depends on noise parameters, simulation results using different $Q(k)$ and $R(k)$, and parameters such as mean error (ME), mean-square error (MSE), and average operation time (AOT) are shown in Table XVI.

Table XVI
COMPARISONS OF THREE FILTERS

$Q^2 = 1, R^2 = 10$	ME	MSE	AOT
EKF	2.2612	16.5732	0.0232
UKF	1.9873	15.7896	0.0563
CKF	1.8287	15.5675	0.0321
$Q^2 = 100, R^2 = 100$	ME	MSE	AOT
EKF	18.3821	35.7246	0.0221
UKF	26.4245	48.7142	0.0589
CKF	20.5632	38.2451	0.0342

The experimental results shown in Table XVI indicate that when the noise parameters are relatively small, accuracy using UKF and CKF methods is slightly better than using EKF. while their time costs are larger than the EKF. The precision and the timeliness of the EKF are superior to the UKF and CKF when the noise parameters are relatively large. Hence, selecting an appropriate filter should be based on the detection environment.

C. NPN linguistic information

For comparison, we employ the fuzzy EKF and the EKF algorithms without the NPN linguistic information. During the process, irrespective of the motion state of the maneuvering target, we use the systemic error parameters shown in Table VIII to describe the tracking of the maneuvering target shown in Fig. 18.

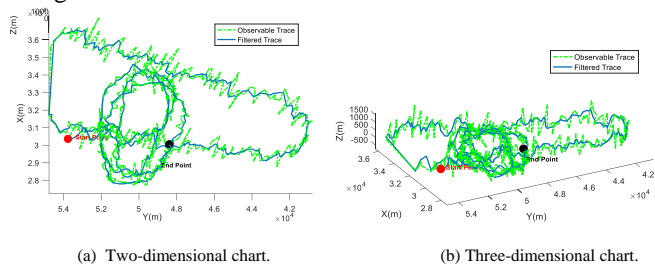(a) Two-dimensional chart.   (b) Three-dimensional chart.

Fig. 18. Tracking with systemic error parameters.

Enlarged sections of the trace with the error parameters before and after the optimization are shown in Fig. 19.

(a) Before optimization (two-dimensions).   (b) After optimization (two-dimensions).

(c) Before optimization (three-dimensions).   (d) After optimization (three-dimensions).
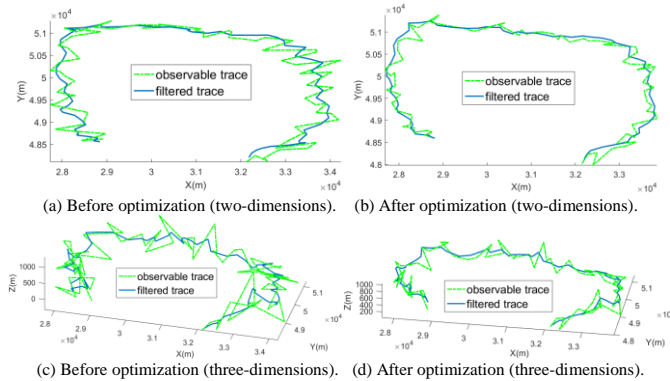
Fig. 19. Trace with error parameters before and after the optimization.

The range of the filtered trace with the systemic error parameters is larger than after the optimization as shown in Fig. 19. The error parameters are reduced using multiple sensors of the maneuvering target. By considering the motion state of the maneuvering target, the systemic error parameters in various phases with the optimized error parameters based on NPNLTSs, are compared in Table XVII.

Table XVII
ERROR PARAMETERS BEFORE AND AFTER OPTIMIZATION

Before (After)	D (D_{op})	α (α_{op})	β (β_{op})
Phases 1	50 (40.4)	0.4 (0.304)	0.4 (0.304)
Phases 2	50 (48.1)	0.4 (0.381)	0.4 (0.381)
Phases 3	60 (58.1)	0.5 (0.481)	0.5 (0.481)
Rate of descent	R_D	R_α	R_β
Phases 1	19.2%	24%	24%
Phases 2	3.8%	4.75%	4.75%
Phases 3	3.17%	3.8%	3.8%

The optimization method using NPNLTSs efficiently reduces the effect of the error in parameter values in various phases and, to a certain extent, improves localization precision. Combined with 1,200 sets of data by three sensors, the errors using the fuzzy EKF algorithm [21] and the EKF algorithms with NPN linguistic information in X, Y, and Z directions are shown in Fig. 20, Fig. 21, and Fig. 22, respectively.
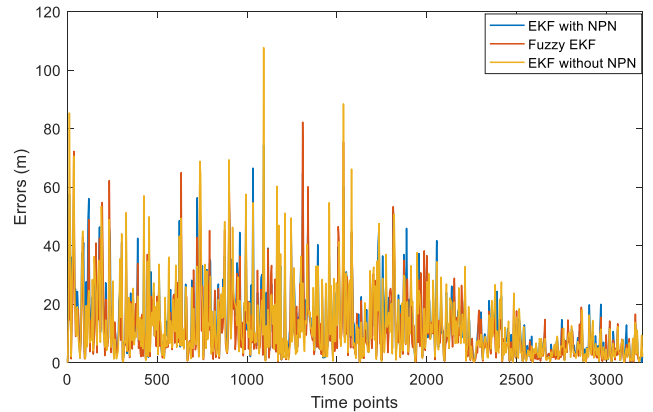

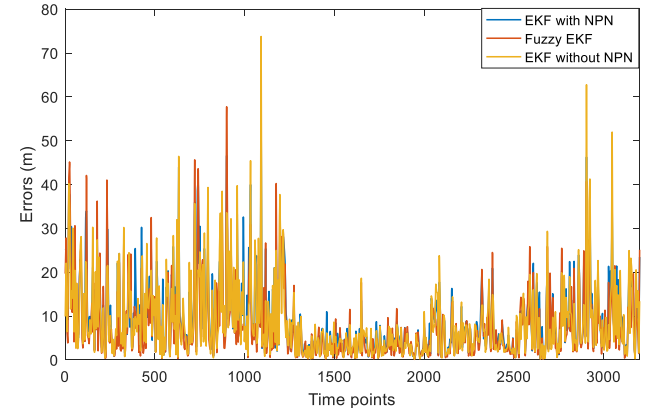Fig. 20. Errors in the X direction.

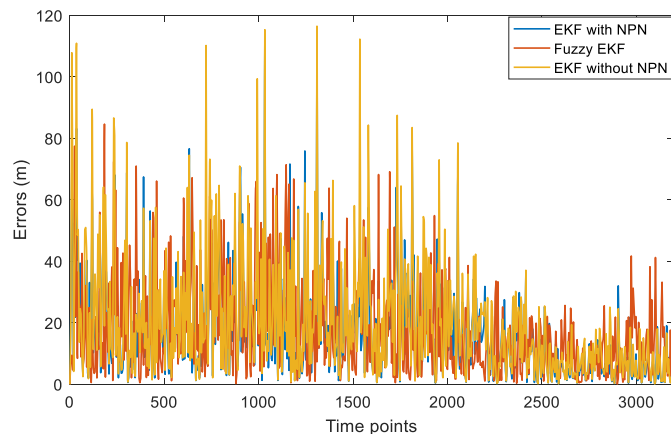

Fig. 21. Errors in the Y direction.

Fig. 22. Errors in the Z direction.

Fig. 20 to Fig. 22 show the errors in X, Y, and Z directions under three situations. The direction in which the greatest average error is in the Z direction, and the smallest average error is in the Y direction. As expected, tracking the maneuvering target using EKF with NPN linguistic information reduces the errors. Compared with the curves in Figs. 15-17, and Figs. 20-22, some parameters are shown in Table XVIII.

Table XVIII
ERROR PARAMETERS USING DIFFERENT METHODS

	ME	MSE	AOT
UKF	1.9873	15.7736	0.0592
CKF	1.8212	15.5865	0.0351
EKF without NPN	2.3634	15.6498	0.0232
Fuzzy EKF	1.6732	13.5621	0.0284
EKF with NPN	1.1528	9.2289	0.0279

The experiment results show that the NPN-EKFTO method improves the accuracy more efficiently than other four methods. The reason may be that NPNLTS considers both quantitative and qualitative information to obtain more precise error parameters. Hence, to some extent, the proposed method reduces the detection errors and could be used in communication, radar, navigation, control, and guidance due to its good systemic performance.

VI. CONCLUSION

Various methods for tracking a maneuvering target such as the EKF, UKF, and CKF algorithms have been proposed to deal with the complexity of the tracking problem. We have proposed the NPN-EKFTO method based on the NPNLTSs and the EKF algorithm. The NPN-EKFTO method optimizes the error parameters by considering the environmental factors and by being combined with the motion state of the maneuvering target at each phase. It may be used to handle complex situations in practice, such as the aircraft commander's emergency decision, dynamic mobile localization in urban area, control of trajectory tracking, and tracking optimization problems of a maneuvering target. It is feasible to use the NPN-EKFTO algorithm in practice.

The method considers the effect of the error parameters with respect to the environmental factors. We have proposed unifying the coordinate system with different SCSs, introduced

data preprocessing of identical recording time using different sensors, and devised the NPN-EKFTO method to solve trace optimization problems. To illustrate the practicability of the proposed method, we have conducted a case study for trace optimization of unknown maneuvering target. We have compared the proposed and the traditional EKF methods and have provided analyses of the results.

Further study of the NPN-EKFTO method may include deriving the weight vector of the evaluation indexes such as analytic hierarchy process with NPNLTSs, considering non-Gaussian noise, and further increasing the number of phases of the maneuvering target in order to improve tracing precision.

REFERENCES

[1] S. P. Puranik and J. K. Tugnait, "Tracking of multiple maneuvering targets using multiscan JPDA and IMM Filtering," *IEEE Trans. Aerosp. Electron. Syst.*, vol. 5, no.1, pp. 4096–4101, 2007.
[2] B. N. Vo, B. T. Vo, and D. Phung, "Labeled random ginite sets and the Bayes multi–target tracking filter," *IEEE Trans. Signal Process.*, vol. 62, no. 24, pp. 6554–6567, 2014.
[3] Q. Hu, H. B. Ji, and Y. Q. Zhang, "Tracking of maneuvering non-ellipsoidal extended target with varying number of sub-objects," *Mech. Syst. Signal Pr.*, vol. 99, pp. 262–284, 2018.
[4] B. P. Larouche and Z. H. Zhu, "Autonomous robotic capture of non-cooperative target using visual servoing and motion predictive control," *Auton. Robot.*, vol. 37, no. 2, pp. 157–167, 2014.
[5] X. Q. Hu, M. Bao, X. P. Zhang, S. Wen, X. D. Li, and Y. H. Hu, "Quantized kalman filter tracking in directional sensor networks," *IEEE Trans. Mobile Comput.*, vol. 17, no. 4, pp. 871–883, 2018.
[6] A. Mohammadzadeh and S. Ghaemi, "Robust synchronization of uncertain fractional-order chaotic systems with time-varying delay," *Nonlinear Dynam.*, vol. 93, no. 4, pp. 1809-1821.
[7] H. Lan, X. Z. Wang, Q. Pan, F. Yang, Z. F. Wang, and Y. Liang, "A survey on joint tracking using expectation-maximization based techniques," *Inf. Fusion*, vol. 30, pp. 52–68, 2016.
[8] D. Bhati, M. Sharma, R. B. Pachori, and V. M. Gadre, "Time–frequency localized three–band biorthogonal wavelet filter bank using semidefinite relaxation and nonlinear least squares with epileptic seizure EEG signal classification," *Digit. Signal Process.*, vol. 62, pp. 259–273, 2017.
[9] W. Y. Li, G. L. Wei, F. Han, and Y. R. Liu, "Weighted average consensus–based unscented Kalman filtering," *IEEE Trans. Cybern.*, vol. 46, no. 2, pp. 558–567, 2016.
[10] D. R. Song, J. Yang, Z. L. Cai, M. Dong, M. Su, and Y. H. Wang, "Wind estimation with a non-standard extended Kalman filter and its application on maximum power extraction for variable speed wind turbines," *Appl. Energ.*, vol. 190, pp. 670–685, 2017.
[11] G. C. Goodwin and K. S. Sin, *Adaptive Filtering Prediction and Control*, Prentice–Hall, Englewood Cliffs, New Jersey, USA 1984.
[12] M. S. Grewal and A. P. Andrews, *Kalman Filtering: Theory and Practice*, Prentice–Hall, New Jersey, 2001.
[13] T. Kailath, A. H. Sayed, and B. Hassibi, *Linear Estimation*, Prentice-Hall, New Jersey, USA 2000.
[14] F. L. Lewis, *Optimal Estimation: With an Introduction to Stochastic Control Theory*, John Wiley and Sons, New York, USA 1986.
[15] D. Simon, *Optimal State Estimation: Kalman, H Infinity and Nonlinear Approaches*, Wiley, Hoboken, New Jersey, 2006.
[16] S. Liu, G. L. Wei, Y. Song, and Y. R. Liu, "Extended Kalman filtering for stochastic nonlinear systems with randomly occurring cyber attacks," *Neurocomputing*, vol. 207, pp. 708–716, 2016.
[17] R. Xiong, F. C. Sun, Z. Chen, and H. W. He, "A data-driven multi-scale extended Kalman filtering based parameter and state estimation approach of lithium–ion polymer battery in electric vehicles," *Appl. Energ.*, vol. 113, pp. 463–476, 2014.
[18] R. Xiong, H. W. He, F. C. Sun, and K. Zhao, "Evaluation on state of charge estimation of batteries with adaptive extended Kalman filter by experiment approach," *IEEE Trans. Veh. Technol.*, vol. 62, no. 1, pp. 108–117, 2013.
[19] I. Arasaratnam and S. Haykin, "Cubature Kalman filters," *IEEE Trans. Automat. Contr.*, vol. 54, no. 6, pp. 1254–1269, 2009.
[20] A. Mohammadzadeh, S. Ghaemi, O. Kaynak and S. Khanmohammadi,

"Observer-based method for synchronization of uncertain fractional order chaotic systems by the use of a general type-2 fuzzy system," *Appl. Soft Comput.*, vol. 49, pp. 544-560.

[21] C. Hu, B. D. Youn, and J. Chung, "A multiscale framework with extended Kalman filter for lithium–ion battery SOC and capacity estimation," *Appl. Energ.*, vol. 92, pp. 694–704, 2012.

[22] H. W. He, R. Xiong, X. W. Zhang, F. C. Sun, and J. X. Fan, "State-of-charge estimation of the lithium–ion battery using an adaptive extended Kalman filter based on an improved Thevenin model," *IEEE Trans. Veh. Technol.*, vol. 60, no. 4, pp. 1461–1469, 2011.

[23] D. Simon, "Training fuzzy systems with the extended Kalman filter," *Fuzzy Sets Syst.*, vol. 132, pp. 189–199, 2002.

[24] J. H. Wang, Y. B. Gao, J. B. Qiu, and C. K. Ahn, "Sliding mode control for non-linear systems by Takagi-Sugeno fuzzy model and delta operator approaches," *Let Control Theory A.*, vol. 11, no. 8, pp. 1205–1213, 2017.

[25] N. Bouzera, M. Oussalah, N. Mezhoud, and A. Khireddine, "Fuzzy extended Kalman filter for dynamic mobile localization in urban area using wireless network," *Appl. Soft Comput.*, vol. 57, pp. 452–467, 2017.

[26] J. Y. Zhang, Y. T. Zhang, and C. Xu, "Backing up a truck on gaussian and non-gaussian impulsive noise with extended Kalman filter and fuzzy controller," *Int. J. Fuzzy Syst.*, vol. 20, no. 3, pp. 791–802, 2018.

[27] K. R. Xia, H. B. Gao, L. Ding, G. J. Liu, Z. Q. Deng, Z. Liu, and C. Y. Ma, "Trajectory tracking control of wheeled mobile manipulator based on fuzzy neural network and extended Kalman filtering," *Neural Comput. Appl.*, vol. 30, no. 2, pp. 447-462, 2018.

[28] X. R. Li and V. P. Jilkov, "Survey of maneuvering target tracking, part I: dynamic models," *IEEE Trans. Aerosp. Electron. Syst.*, vol. 39, no. 4, pp. 1333–1364, 2003.

[29] X. R. Li and V. P. Jilkov, "Survey of maneuvering target tracking, part II: motion models of ballistic targets," *IEEE Trans. Aerosp. Electron. Syst.*, vol. 46, no. 1, pp. 96–119, 2010.

[30] Z. S. Xu, "A method based on linguistic aggregation operators for group decision making with linguistic preference relations," *Inform. Sciences*, vol. 166, no. 1–4, pp. 19–30, 2004.

[31] R. M. Rodriguez, L. Martinez, and F. Herrera, "Hesitant fuzzy linguistic term sets for decision making," *IEEE Trans. Fuzzy Syst.*, vol. 20, pp. 109–119, 2012.

[32] Q. Pang, H. Wang, and Z. S. Xu, "Probabilistic linguistic term sets in multi-attribute group decision making," *Inform. Sciences*, vol. 369, pp. 128–143, 2016.

[33] L. A. Zadeh, "The concept of a linguistic variable and its application to approximate reasoning-I," *Inform. Sciences*, vol. 8, no. 3, pp. 199–249, 1975.

[34] Y. X. Zhang, Z. S. Xu, H. Wang, and H. C. Liao, "Consistency-based risk assessment with probabilistic linguistic preference relation," *Appl. Soft Comput.*, vol. 49, pp. 817–833, 2016.

[35] H. C. Liao, L. S. Jiang, and Z. S. Xu, "A linear programming method for multiple criteria decision making with probabilistic linguistic information," *Inform. Sciences*, vol. 415, pp. 341–355, 2017.

[36] Y. X. Zhang, Z. S. Xu, and H. C. Liao, "A consensus process for group decision making with probabilistic linguistic preference relations," *Inform. Sciences*, vol. 414, pp. 260–275, 2017.

[37] X. X. Wang, Z. S. Xu, and X. J. Gou, "Nested probabilistic-numerical linguistic term sets in two-stage multi-attribute group decision making," *Appl. Intell.*, 2019, DOI: 10.1007/s10489-018-1392-y.

[38] X. X. Wang, Z. S. Xu, and X. J. Gou, "Distance and Similarity Measures for Nested Probabilistic-Numerical Linguistic Term Sets Applied to Evaluation of Medical Treatment," *Int. J. Fuzzy Syst.*, 2019, DOI: 10.1007/s40815-019-00625-x).

[39] X. X. Wang, Z. S. Xu, and X. J. Gou, "Consensus-Based Track Association with Multi-Static Sensors under Nested Probabilistic-Numerical Linguistic Environment," Technical Report, 2019.

Xinxin Wang received the Bachelor's degree and Master's degree from Southwest Petroleum University, Chengdu, China, in 2014 and 2017, respectively. She is currently working toward the Ph.D. degree in Business School, Sichuan University, China. Her research interests include decision analysis, optimization, computing with words. She has published more than 10 peer reviewed papers, and her research works has been published in *Applied Intelligence*, *International Journal of Fuzzy Systems*, and *Fuzzy Systems and Mathematics*, etc. She has received numerous honors and awards, including the First Prize in National Post-Graduate Mathematical Contest in Modeling in 2015 and 2016, the 2015 and 2016 National scholarship for graduate students, etc.

Zeshui Xu (M'08-SM'09-F'19) received the Ph.D. degree in management science and engineering from Southeast University, Nanjing, China, in 2003. He is a Distinguished Young Scholar of the National Natural Science Foundation of China and the Chang Jiang Scholars of the Ministry of Education of China. He is currently a Professor with the Business School, Sichuan University, Chengdu. He has been selected as a 2014-2018 Highly Cited Researcher in the fields of Computer Science and Engineering, and selected as the most cited Chinese researchers (Ranked first in Computer Science, 2014-2018, Released by Elsevier). His h-index is 114. Prof. Xu is the Associate Editor of *IEEE Transactions on Fuzzy Systems, Information Sciences, Fuzzy Optimization and Decision Making, International Journal of Fuzzy Systems, International Journal Machine Leaning and Cybernetics, etc.*, and the Editorial (Advisory)Member of more than thirty professional journals, including *Knowledge-Based Systems, Information Fusion, Technological and Economic Development of Economy, Applied Intelligence, etc.*

Xunjie Gou is now pursuing his Ph.D. degree in both Management Science and Engineering at Sichuan University, Sichuan, China, and Information and Communication Technology at University of Granada, Granada, Spain. He has published more than 20 peer reviewed papers, many in high-quality international journals including *Knowledge-Based Systems, Information Sciences*, *Information Fusion*, etc. His current research interest includes large scale group decision making, double hierarchy linguistic term set, computing with words, etc.

Ljiljana Trajkovi´c (S'78–M'86–F'05) received the Dipl.Ing. degree from the University of Pristina, Pristina, Yugoslavia, in 1974, the M.Sc. degrees in electrical engineering and computer engineering, both from Syracuse University, Syracuse, NY, USA, in 1979 and 1981, respectively, and the Ph.D. degree in electrical engineering from the University of California, Los Angeles, Los Angeles, CA, USA, in 1986. She is currently a Professor with the School of Engineering Science, Simon Fraser University, Burnaby, BC, Canada. From 1995 to 1997, she was a National Science Foundation Visiting Professor with the Electrical Engineering and Computer Sciences Department, University of California, Berkeley, Berkeley, CA, USA. She was a Research Scientist with Bell Communications Research, Morristown, NJ, USA, from 1990 to 1997 and a Technical Staff Member with AT&T Bell Laboratories, Murray Hill, NJ, USA, from 1988 to 1990. Her current research interests include high-performance communication networks, control of communication systems, computer-aided circuit analysis and design, and theory of nonlinear circuits and dynamical systems. Dr. Trajkovi´c serves as the President of the IEEE Systems, Man, and Cybernetics Society (2014–2015) and has served as the President-Elect (2013), the Vice President Publications (2010 to 2011 and 2012 to 2013), the Vice President Long-Range Planning and Finance (2008 to 2009), a member of the Board of Governors (2004 to 2006). She is a Chair of the IEEE Circuits and Systems Society Joint Chapter of the Vancouver/Victoria Sections.